Inorganic Chemistry

Article

pubs.acs.org/IC

How the Surface Structure Determines the Properties of CuH

Elliot Bennett,[†] Thomas Wilson,[†] Patrick J. Murphy,[†] Keith Refson,[‡] Alex C. Hannon,[§] Silvia Imberti,[§] Samantha K. Callear,[§] Gregory A. Chass,[∥] and Stewart F. Parker*[,§]

[†]School of Chemistry, Bangor University, Bangor LL57 2UW, U.K.

[‡]Computational Science and Engineering Department and [§]ISIS Facility, STFC Rutherford Appleton Laboratory, Chilton, Didcot OX11 0QX, U.K.

[∥]School of Biological and Chemical Sciences, Queen Mary University of London, London E1 4NS, U.K.

Supporting Information

ABSTRACT: CuH is a material that appears in a wide diversity of circumstances ranging from catalysis to electrochemistry to organic synthesis. There are both aqueous and nonaqueous synthetic routes to CuH, each of which apparently leads to a different product. We developed synthetic methodologies that enable multigram quantities of CuH to be produced by both routes and characterized each product by a combination of spectroscopic, diffraction and computational methods. The results show that, while all methods for the synthesis of CuH result in the same bulk product, the synthetic path taken engenders differing surface properties. The different behaviors of CuH obtained by aqueous and nonaqueous routes can be ascribed to a combination of very different particle size and dissimilar surface termination, namely, bonded hydroxyls for the aqueous routes and a coordinated donor for the nonaqueous routes. This work provides a particularly clear example of how the nature of an adsorbed layer on a nanoparticle surface determines the properties.

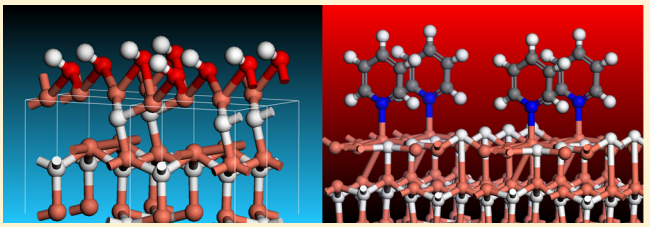

INTRODUCTION

Copper(I) hydride, CuH, was first prepared by Würtz[1] in 1844. It is unique among the binary metal hydrides in that it can be synthesized in solution, at room temperature. CuH appears in varied circumstances: it is observed as an intermediate phase in the dissolution of brass in sulfuric acid[2,3] and electroless copper plating.[4] CuH is proposed[5] as the means by which hydrogen is stored subsurface in $Cu/Zn/Al_2O_3$ methanol synthesis catalysts, and it is suggested as a route to copper catalysts.[6] In recent years, soluble derivatives of CuH prepared by nonaqueous routes have become important as mild reducing agents.[7−9] One such compound, Stryker's reagent $[HCu(PPh_3)]_6$,[10] is widely used and by appropriate choice of conditions can be made catalytic in action.[9]

Würtz prepared CuH by the reaction of aqueous copper sulfate with hypophosphorous acid (eq 1). This remains the most established[11,12] method of preparation, although several other routes have been developed including reduction of aqueous Cu^{2+} by borohydride ion[13] (eq 2) and precipitation of the hydride from pyridine solutions[14,15] of CuI and $LiAlH_4$ (eq 3). Very recently a sonochemical synthesis[16] (eq 1a) was reported, which results in a product very similar to that obtained from the Würtz route (eq 1).

$$4Cu^{2+}_{(aq)} + 6H_2PO_2^-{}_{(aq)} + 6H_2O \rightarrow 4CuH_{(ppt)} + 6H_2PO_3^-{}_{(aq)} + 8H^+_{(aq)} \quad (1)$$

$$Cu^{2+}_{(aq)} + \text{ultrasound} \rightarrow CuH_{(ppt)} \quad (1a)$$

$$2Cu^{2+}_{(aq)} + 2BH_4^-{}_{(aq)} + 6H_2O \rightarrow 2CuH_{(ppt)} + 2B(OH)_{3(ppt)} + 2H^+_{(aq)} + 5H_{2(g)} \quad (2)$$

$$3CuI_{(pyridine)} + LiAlH_{4(ether)} \rightarrow 3CuH_{(pyridine)} + AlI_{3(ppt)} + LiH_{(ppt)} \quad (3)$$

One of the fascinating characteristics of CuH is that aqueous and nonaqueous synthetic routes apparently give differing products. The insoluble CuH produced by (route 1) ("CuH/Würtz") is readily hydrolyzed by base and has a "shell" of water that is essential to its stability, the removal of which is reported[12] to result in the immediate explosive decomposition of the hydride. CuH produced by this route has a well-defined structure that has been determined by X-ray[17,18] and neutron diffraction.[18] Binary metal hydrides usually have the same crystal structure as the pure metal but with a degree of lattice expansion to accommodate the interstitial hydrides.[19] CuH is unusual in that it has the Würtzite structure rather than the face centered cubic (fcc) structure of copper metal; the water shell is apparently amorphous as no diffraction features were observed.

Received: November 11, 2014
Published: February 11, 2015

DOI: 10.1021/ic5027009
Inorg. Chem. 2015, 54, 2213−2220

(An fcc form of CuH can be obtained by direct reaction of the elements, but this is only stable above 12.5 GPa.)[20]

Route (2) also results in an insoluble form of CuH ("CuH/$[BH_4]^-$"), and in this case the precipitate is coffee-colored[13] rather than the rust-red of route (1) or blood-red of route (3).

Route (3) is a nonaqueous path that results in a form of CuH ("CuH/pyridine") that is soluble in "soft" donor solvents, including alkylphosphines, phosphites, alkyl sulfides, and pyridines.[15] The product from this route contains 4−20 wt % pyridine with a much smaller particle size of ∼10 nm rather than the hundreds of nanometers from route (1). It is speculated[15] that this may be why it is soluble.

Spectroscopic investigations of the products of the various methods of producing CuH have been inconclusive. Attempts to record infrared and Raman spectra from the CuH/Würtz product were generally unsuccessful;[21,22] however, a recent investigation[23] observed broad infrared bands in the range of 700−1200 cm^{-1}. The CuH/pyridine product has been stated to not yield infrared or Raman spectra.[15] More recently, infrared bands at 522, 1272, and 1656 cm^{-1} have been reported.[22] These were assigned as the Cu−H stretch, Cu−H bend, and Cu−N stretch, respectively; however, assignment of the 1272 and 1656 cm^{-1} bands to coordinated[24] pyridine would appear more plausible.

In the nearly 200 years since its discovery, CuH has been investigated many times. The most comprehensive study[12] was Warf and Feitknecht's 1950 work on the product from the Würtz route and was restricted to powder X-ray diffraction (XRD) and wet chemistry methods of analysis. A more recent investigation[25] using largely powder XRD and transmission electron microscopy arrived at generally similar conclusions regarding the stability of the material. Apart from the initial reports, the nature of the CuH/$[BH_4]^-$[13]and CuH/pyridine[14] products has been sparsely investigated.

Two key questions concerning CuH are still unanswered: do the aqueous and nonaqueous routes result in the same material, and how does the residual solvent interact with the bulk? We developed multigram scale syntheses of the materials that have enabled us to use a combination of computational, structural, and spectroscopic methods to provide insight into these questions.

MATERIALS AND METHODS

Sample Preparation. Neutron techniques typically require several grams of sample for successful investigations. We modified the literature syntheses of CuH/Würtz[5] and CuH/pyridine[14] (eqs 1 and 3) to prepare the semimacro quantities required. Detailed descriptions of the procedures are given in the Supporting Information. In all cases exclusion of air is essential. Drying of the CuH/Würtz product was done under flowing helium in a sealed metal can. ***Caution!*** *The dried product may decompose explosively.*

Neutron Diffraction. Total scattering time-of-flight neutron diffraction (ND) measurements were performed using the diffractometer, SANDALS,[26] at ISIS.[27] Powder CuH samples prepared by the aqueous and nonaqueous routes were loaded into flat-plate sample holders of 40 mm diameter and 1 mm or 2 mm thickness made of the null scattering alloy Ti(52.5%)Zr(47.5%). A full set of experimental corrections and an absolute normalization were made using the standard Gudrun[28] and ATLAS[29] software. The diffractograms were analyzed using the PDFgui program.[30]

X-ray Diffraction. In an argon-purged glovebag, CuH samples prepared by the three routes were loaded into silica glass capillaries of internal diameter 1.0 mm. XRD measurements were made using a Panalytical X'Pert Pro Multipurpose Diffractometer, running in capillary mode, with a silver anode source (wavelength 0.560 885 Å). Measurements were also made on an empty capillary and the empty instrument.

Inelastic Neutron Scattering Spectroscopy. Inelastic neutron scattering (INS) spectroscopy is a complementary form of vibrational spectroscopy,[31] where the scattering event is between a neutron and an atomic nucleus; thus, the electronic nature of the material, whether conductor, semiconductor, or insulator, is irrelevant. The scattering intensity depends on the incoherent inelastic scattering cross section and the amplitude of vibration. For ^1H both of these are large; consequently, the scattered intensity is dominated by hydrogenous motion. Neutrons are highly penetrating, so the spectra are representative of the bulk rather than just the surface. INS spectra were recorded with the spectrometers TOSCA[31,32] and MAPS[33,34] at ISIS.[27] The operating principles of the two instruments are described in detail elsewhere.[31,34] The instruments are complementary, and for the present work, the feature of interest is that TOSCA provides high resolution in the region of 24−2000 cm^{-1}, whereas MAPS enables access to the 2000−5000 cm^{-1} spectral region. For the measurements, the CuH samples were loaded (in an Ar-flushed glovebag) into sealed aluminum cans, or the samples in the TiZr cans measured on SANDALS were used. In either case, the sample cans were then loaded into a closed cycle cryostat and cooled to ∼20 K, and then the spectra were recorded for 8−12 h to generate spectra of sufficient quality.

Computational Methods. Periodic density functional theory (periodic-DFT) calculations were carried out using a plane-wave basis-set and pseudopotentials as implemented in the CASTEP code.[35,36] Initial input structures were generated from the CuH structure as determined by neutron diffraction.[18] For the nonstoichiometric $CuH_{0.75}$ structure, one hydrogen atom was removed from a 2 × 1 × 1 supercell. Test calculations with spin-polarized structures showed no unpaired electrons, so all subsequent calculations assumed spin-paired structures. Calculations of the adsorbed species on the surface of $CuH_{0.75}$ used a five-layer slab generated from the optimized bulk structure with a 10 Å vacuum gap. The generalized gradient approximation Perdew−Burke−Ernzerhof (PBE) functional was used in conjunction with optimized norm-conserving pseudopotentials with a plane-wave cutoff energy of 880 eV. Electronic densities of states were generated from a subsequent band-structure calculation using OptaDOS.[37] Phonon modes were calculated using density-functional perturbation theory.[38] As a prerequisite to any lattice dynamics calculation a full geometry optimization of the internal atomic coordinates was performed. The output of the phonon calculation includes infrared intensities and the atomic displacements of the atoms in the mode. The visualizations of the Cartesian nature of these modes were carried out in Materials Studio (Accelrys),[39] and the INS spectra were generated with ACLIMAX.[40] We emphasize that the transition energies were not scaled.

RESULTS

Computational Studies. A calculation using the experimental structure determined by neutron diffraction[18] showed that CuH is a stable structure, with no imaginary modes as shown by the dispersion curves, Supporting Information, Figure S2. As noted previously,[23] stoichiometric CuH exhibits a band gap of ∼0.74 eV and thus is not a metal, Supporting Information, Figure S3. Given the well-known underestimation of the band gap by periodic-DFT, this is likely to be a lower estimate, and the material is either a semiconductor or an insulator.

The literature shows that CuH is often nonstoichiometric: compositions of $CuH_{0.89}$ and $CuD_{0.91}$ prepared by the Würtz method and characterized by diffraction were reported in 1955,[18] while samples prepared by the pyridine route had a ratio of H to total Cu from 0.58 and 0.96 and an average of 0.81.[15] To see what effect the nonstoichiometry would have, a 2 × 1 × 1 supercell was created, and one of the hydrogen atoms was removed to generate Cu_4H_3, that is, $CuH_{0.75}$, creating a

DOI: 10.1021/ic5027009
Inorg. Chem. 2015, 54, 2213−2220

monoclinic cell, space group *Pm* (No. 6). A spin-polarized geometry optimization, with the lattice fixed at the experimental parameters, showed that the structure was diamagnetic and that it exhibited a large negative pressure, indicating that the stable form had a smaller unit cell. In a second (not spin-polarized) optimization, all the lattice angles were fixed, but the cell lengths and contents were allowed to optimize. This calculation resulted in a small, 7.4%, contraction of the unit cell (initial volume = 67.59 Å^3, final volume = 62.93 Å^3) with real modes across the entire Brillouin zone, Supporting Information, Figure S4. Inspection of the dispersion curves and the electronic density of states showed that the nonstoichiometric material was metallic, Figure S3.

CuH/Würtz. The Cu−H distance can be observed directly via the radial distribution function (rdf), $D(R)$, generated from total scattering neutron diffraction data. Hydrogen, ^{1}H, has a negative scattering length, whereas deuterium, carbon, nitrogen, and copper have positive scattering lengths. (A negative scattering length means that the neutron undergoes a 180° phase shift on scattering.) Thus, negative-going features are distances that involve hydrogen.

Contrary to the literature,[12,17] it proved possible to dry the product in a stream of dry helium gas at room temperature without significant decomposition. Figure 1a shows the pattern

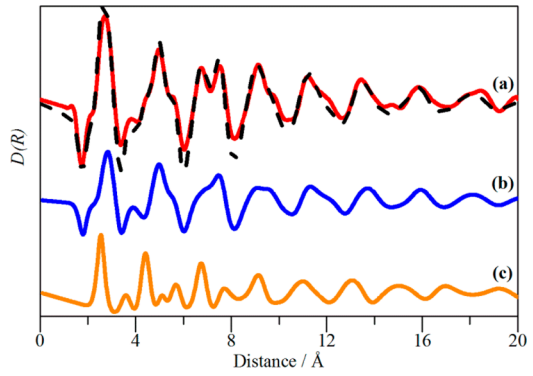

Figure 1. Total scattering neutron diffraction patterns of (a) CuH/Würtz after drying, (b) $CuH_{0.75}$, and (c) Cu metal. The dashed line in (a) is a fit to the data assuming a composition of Cu metal to $CuH_{0.75}$ in a ratio of 1:1.65; (b, c) were generated from the crystal structures.

obtained from the dried product. The negative-going peak at 1.73 Å is characteristic of, and diagnostic of, Cu−H. The powder XRD pattern showed the presence of CuH and the known[11,12] decomposition products Cu_2O and Cu metal (Supporting Information, Figure S5). Also shown in Figure 1a (dashed line) is a fit to the data as a sum of the $CuH_{0.75}$ structure (Figure 3b) and Cu metal (Figure 3c) in a ratio of 1.65:1. Fits using a mixture of Cu and stoichiometric CuH were generally inferior, refining the hydrogen occupancy obtained from the dried product producing values of ∼0.75.

Figure 2a shows the INS spectrum of H_2O ice I_h, and Figure 2b shows that of the product of the Würtz route. It can be seen that the spectra are very similar below 750 cm^{-1}, consistent with the presence of water in the product. It is surprising that this is present as an ordered form of ice, rather than the disordered layers commonly found on both transition metal and main group hydrous metal oxides such as $PdO{\cdot}H_2O$,[41] $Co_3O_4{\cdot}xH_2O$,[42] $SnO_2{\cdot}xH_2O$[43], and $Al_2O_3{\cdot}xH_2O$.[44] There is a clear difference between the two spectra at ∼1100 cm^{-1} suggesting an additional peak is present in the product. Figure

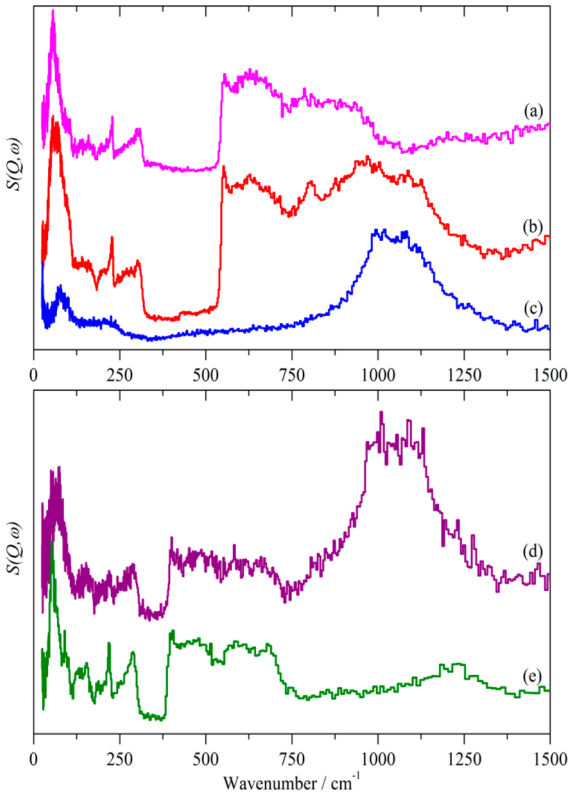

Figure 2. INS spectra recorded on TOSCA at 20 K of (a) H_2O ice I_h, (b) the product of the Würtz route, (c) the same sample as (b) after drying, (d) the product of the Würtz route after exchange with D_2O, and (e) D_2O ice I_h.

2c shows the result after drying, and a broad, structured feature is revealed centered at ∼1050 cm^{-1}. We assign this peak to CuH. An additional peak that is present at ∼2100 cm^{-1} (not shown) is assigned as the first overtone of the 1050 cm^{-1} peak.

In a separate experiment, the product was prepared in the same way by the Würtz route and then stirred in excess D_2O overnight before isolation. The result is shown in Figure 2d (without drying) and the INS spectrum of D_2O ice I_h in 2e. Comparison of Figure 2d,e shows that crystalline D_2O ice I_h. is present. However, the much smaller total scattering cross section of deuterium (^{1}H = 82.03 barn, ^{2}H = 7.64 barn, 1 barn = 1 × 10^{-28} m^2) means that the CuH peak is visible. The ready exchange of H_2O for D_2O, without affecting the CuH, strongly supports a core−shell model.

CuH is known to be unstable,[11,12,25] and this was also found to be the case here. The D_2O-exchanged sample was stored in a sealed (but not completely airtight) can and kept at room temperature. It was measured one, four, and six days after preparation and had almost completely decomposed by the sixth day, Supporting Information, Figure S6.

Figure 3 compares the INS spectrum of the dried material, which strongly resembles that of many hydrogen-in-metal systems,[19] with the spectra generated from the $CuH_{0.75}$ and CuH calculations. The structure present in the main feature, at 1050 cm^{-1} for both calculations, is barely present in the experimental spectrum; this is perhaps to be expected since the real material may well exhibit a range of stoichiometry. INS spectroscopy is sensitive to modes across the complete Brillouin zone, whereas infrared and Raman spectra only occur at the Γ-point. Inspection of the dispersion curves for

DOI: 10.1021/ic5027009
Inorg. Chem. 2015, 54, 2213−2220

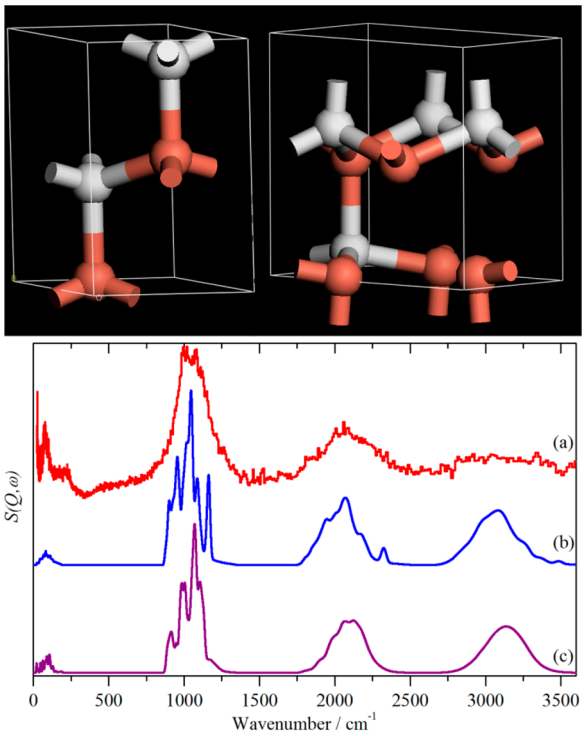

Figure 3. INS spectra recorded on TOSCA at 20 K of (a) the product of the Würtz route after drying, (b) calculated for nonstoichiometric $CuH_{0.75}$ (upper structure on right), and (c) calculated for stoichiometric CuH (structure on left above).

CuH and $CuH_{0.75}$ (Figures S2 and S4) shows that the Cu−H stretch modes are significantly dispersed (bands are not flat) and that they occur in the range of 900−1150 cm^{-1}. The INS spectrum is generated from the dispersion curves by projecting them onto the wavenumber axis, which results in a broad band that crests where the curves are densest, at ∼1050 cm^{-1}, as seen experimentally. Overall, the agreement is marginally better with $CuH_{0.75}$. This is also the case for the ND and XRD data, Figure 1 and Supporting Information, Figure S5, respectively, indicating that the material is nonstoichiometric, consistent with the literature.

CuH/Pyridine. The XRD diffractogram of CuH/pyridine, Supporting Information, Figure S7, shows that CuH is clearly present. The width of the experimental features is striking, and a crude estimate of the scattering domain size from the Scherrer equation indicates ∼13 Å. (Note that this is not necessarily the particle size, since an agglomerate of particles of this size would give the same result.) This is much smaller than the ∼100 Å previously suggested.[15] The width of the features precludes a definitive choice between stoichiometric and nonstoichiometric CuH, although previous work[15] favors the latter. This also appears to be a much cleaner route to CuH since there is no evidence for the Cu metal and Cu_2O impurities found in the Würtz preparation.

Room-temperature ND data confirm and extend these conclusions. Figure 4a compares the rdfs for liquid pyridine (green) and the CuH/pyridine sample. As expected for a liquid, only short-range (<10 Å) correlations are found for pure pyridine. For the CuH/pyridine sample, the correlations extend further in distance but are absent beyond 20 Å consistent with the XRD data. A negative-going peak at 1.75 Å confirms the presence of CuH in the sample. Figure 4b shows a comparison of the scaled difference data: ([CuH/pyridine] − [pyridine])

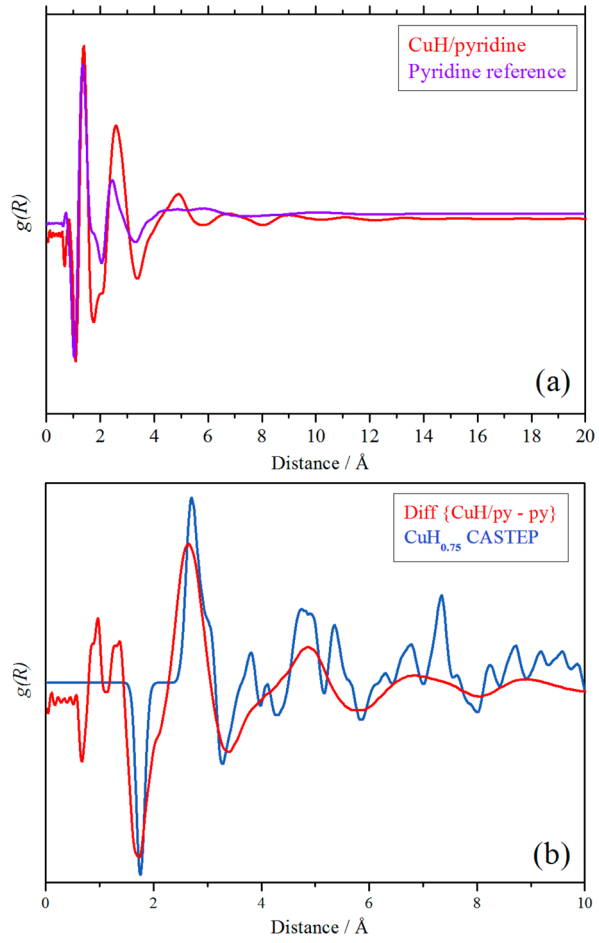

Figure 4. Comparison of the radial distribution functions of (a) the product of the pyridine route (red) and liquid pyridine (purple) and (b) the scaled difference data: ([CuH/pyridine] − [pyridine]) (red) and $CuH_{0.75}$ (blue).

and the rdf for the $CuH_{0.75}$ model and shows reasonable agreement.

The INS spectrum of the CuH/pyridine product is compared to that of solid pyridine in Figure 5 and also to that of a model compound, tetrakispyridine copper(II) triflate, [Cu-

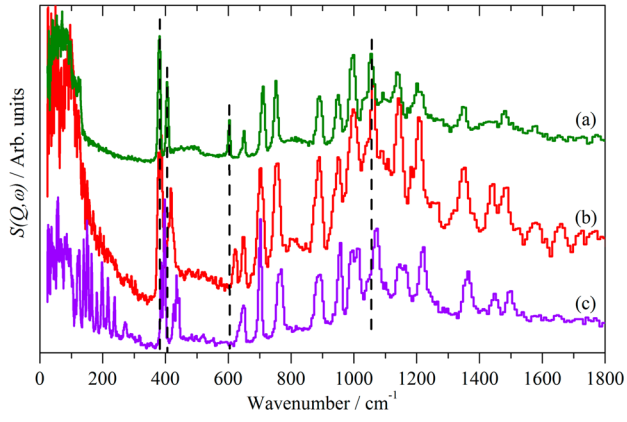

Figure 5. INS spectra of (a) solid pyridine C_5H_5N, (b) the CuH/pyridine product, and (c) $[Cu(C_5H_5N)_4(SO_3CF_3)_2]$. All spectra were recorded on TOSCA at 20 K. The vertical dashed lines indicate pyridine modes that undergo a significant shift on coordination.

DOI: 10.1021/ic5027009
Inorg. Chem. 2015, 54, 2213−2220

$(C_5H_5N)_4(SO_3CF_3)_2]$. For the CuH/pyridine product, several of the modes are seen to shift in energy, consistent with coordination[24] to copper. The shifts are similar to those commonly found in metal−pyridine complexes[24] and about half those of pyridine coordinated to a strongly acidic site on alumina.[45] Supporting Information, Table S1 gives the transition energies for selected modes of pyridine as a solid and bound to CuH.

Comparison of the three spectra suggests that the Debye−Waller factor is pyridine > CuH/pyridine > $[Cu(C_5H_5N)_4(SO_3CF_3)_2]$, as judged by the relative ratios of the ν_{16a} ring torsion mode at ∼390 cm^{-1} and the ν_{18b} ring stretch mode at ∼1060 cm^{-1}. (On TOSCA, the effect of the Debye−Waller factor is to reduce the intensity of modes, rising with increasing energy transfer.) This order would be consistent with the expected strength of the intermolecular bonding in the three materials: van der Waals < coordination to Cu^+ < coordination to Cu^{2+}. The progressive shift to higher energy of the highlighted modes in Figure 5 also supports this view.

The spectrum of $[Cu(C_5H_5N)_4(SO_3CF_3)_2]$ is clearly similar to, but not identical to, that of CuH/pyridine. A major difference is that there are a large number of discrete modes in the range of 100−200 cm^{-1}, whereas for CuH/pyridine a continuum is found. A periodic-DFT calculation of $[Cu(C_5H_5N)_4(SO_3CF_3)_2]$ (Supporting Information, Figure S8) shows that these correspond to the frustrated translations and rotations of the coordinated pyridine (and triflate, although these are generally of low intensity because of the very small scattering cross section of SO_3CF_3) ligands. The continuum seen for CuH/pyridine suggests that the pyridine is similarly bound but is strongly disordered on the CuH surface.

In contrast to the aqueous routes, the CuH/pyridine product does not show the clear signature of the Cu−H stretch, which is a strong fundamental and pronounced overtones. To observe these, the deuterated pyridine (pyridine-D5) product was prepared by dissolution of the CuH/pyridine product in pyridine-D5 and subsequently reprecipitated. Neutron diffraction showed the presence of Cu−H, and Figure 6 shows the INS spectrum after subtraction of pyridine-D5, baseline correction (Supporting Information, Figure S9 shows the process), and curve-fitting. The peaks occur at the same transition energies as for CuH/Würtz, but the width of the fundamental is approximately twice that found for the product of the aqueous route.

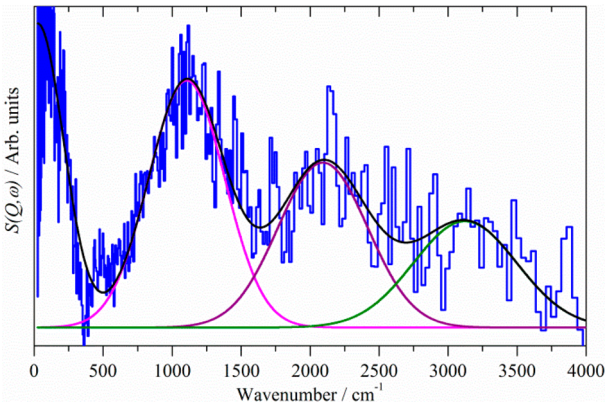

Figure 6. Curve resolution of the INS spectrum of CuH/pyridine-D5 (after subtraction of pyridine-D5 and baseline correction) showing the strong fundamental and pronounced overtones of the Cu−H stretch.

DISCUSSION

The structural and spectroscopic data presented here admit only one conclusion: irrespective of the method of preparation the CuH product is the same, and all the product materials have the hexagonal lattice identified in relevant historic structure determinations.[17] The differences between the products obtained from the aqueous and nonaqueous routes are significant, especially the capacity for dissolution. It has been previously noted[15] that there is a marked difference in particle size depending on the method of synthesis as evidenced in our XRD data (Figures S5 and S7). However, this does not explain the difference in behavior.

The INS spectrum in the high-energy region of CuH/Würtz after drying is shown in Figure 7. Curve fitting shows the

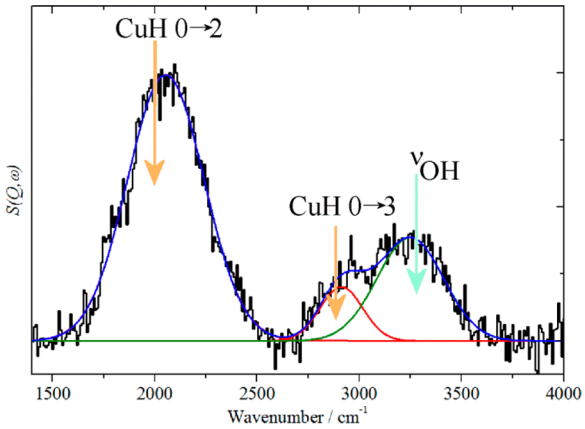

Figure 7. Curve-resolved (after baseline correction) INS spectrum of the dried CuH/Würtz product in the high-energy region recorded on MAPS (with an incident energy of 4840 cm^{-1}) at 20 K. Note the absence of any peak at ∼1600 cm^{-1}.

presence of peaks at 2054, 2912, and 3249 cm^{-1}. INS spectroscopy is intrinsically a two-dimensional form of spectroscopy, in that the measured intensity $S(Q,\omega)$ depends on both the energy transfer (ω, cm^{-1}) and the momentum transfer (Q, $Å^{-1}$). As shown elsewhere,[46] the value of Q at which $S(Q,\omega)$ is a maximum, Q_{max}, depends on the order n of the transition; n = 1 for a fundamental, n = 2 for a first overtone or binary combination, n = 3 for a second overtone or ternary combination, etc., and Q_{max} increases with increasing n. From the map of $S(Q,\omega)$, shown in Figure 8, it is clear that Q_{max} progressively increases for the transitions at 1060, 2054, and 2912 cm^{-1}, indicating that they correspond to the n = 1, 2, 3 transitions of CuH. From the n = 1 and 2 transitions and the usual expressions for the energy levels of an anharmonic oscillator,[47] the harmonic frequency ω_e and the anharmonicity term $2\omega_e x_e$ are determined to be 1122 and 66 cm^{-1}, respectively; hence, the n = 3 transition is predicted at 2970 cm^{-1} in fair agreement with the 2912 cm^{-1} found experimentally.

The only reasonable assignment for the 3249 cm^{-1} peak is to the O−H stretch of a surface hydroxyl group. The possibility that it is due to residual water can be eliminated as there is no feature at ∼1600 cm^{-1} where the water-scissoring (angle-bend) mode would occur. To test whether hydroxyls are stable on the surface of CuH, a five-layer slab cleaved along (001) was created from the geometry-optimized structure of $CuH_{0.75}$ and the exposed copper atoms capped with hydroxyls. The structure is stable and predicts O−H stretch modes at 3300−

DOI: 10.1021/ic5027009
Inorg. Chem. 2015, 54, 2213−2220

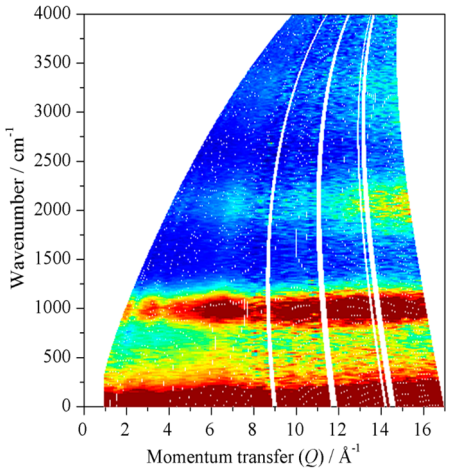

Figure 8. $S(Q,\omega)$ map of the dried CuH/Würtz product recorded on MAPS at 20 K with an incident energy of 4840 cm^{-1}.

3450 cm^{-1} and Cu−O−H bending modes in the 500−800 cm^{-1} region. Figure 9 shows a comparison of the experimental

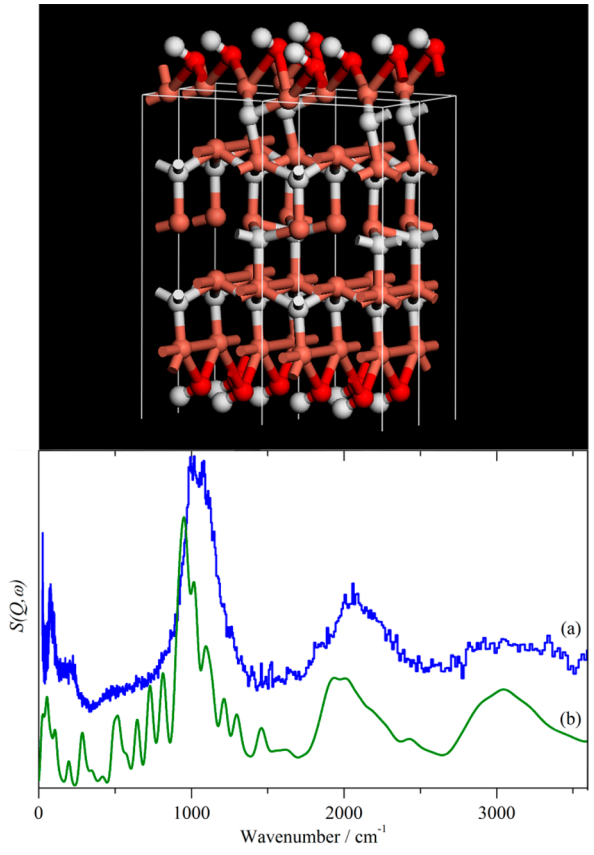

Figure 9. Comparison of the INS spectrum of (a) the dried CuH/Würtz product and (b) that generated from the hydroxyl-capped five-layer slab of $CuH_{0.75}$ shown in the upper part of the figure.

spectrum of the dried material (Figure 9a) and that generated from the calculation (Figure 9b). The relative intensities of the Cu−H and Cu−O−H bending modes are mismatched when compared with the experimental spectrum; however, the ratio of CuH to OH is 4:1 in the calculation, whereas in reality it will be much greater since the particles are relatively large. To model this would require a much thicker slab with many more atoms, and this is beyond our computational resources. The O−H stretch modes are in reasonable agreement with the experimental result, although this is probably the fortuitous[48] result of the cancellation of errors caused by the overestimation of the O−H bond length that results from the use of the PBE functional and the neglect of anharmonicity. The bending modes would account for the tailing to low-energy transfer seen in Figure 9a, which is not predicted by the calculations on bulk CuH and $CuH_{0.75}$ (Figure 3b,c).

It has been previously suggested[25] that a layer of CuOH·nH_2O[49] that forms over time is responsible for the slower decomposition of CuH/Würtz in water than air. Our results demonstrate that hydroxyls are present at the surface but are forming during the reaction sequence and that they are probably present as a terminating monolayer rather than as an encapsulating shell. We note that the hydroxyl layer is stable in the absence of water (Figure 7).

For CuH/pyridine there is neither an obvious route to hydroxyl formation, since it is a nonaqueous synthesis under an inert atmosphere, nor any spectroscopic evidence for hydroxyls, Figure 10. The INS spectrum, Figure 5, provides clear evidence

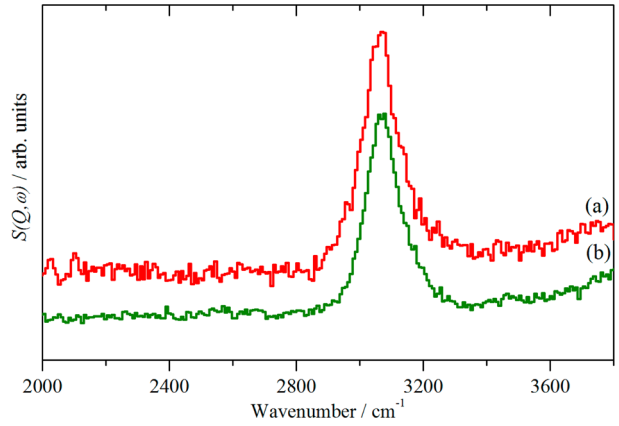

Figure 10. INS spectrum in the high-energy region recorded on MAPS (with an incident energy of 4840 cm^{-1}) at 20 K of (a) the CuH/pyridine product and (b) pyridine. Note that there is no evidence for an O−H stretch mode in (a).

for coordination of pyridine to copper. It is also noteworthy that *all* the pyridine is coordinated as shown by the absence of the ν_{6a} mode at 604 cm^{-1} in the CuH/pyridine product; rather, the ν_{6a} mode has shifted to 621 cm^{-1}. This suggests a model of a core of nonstoichiometric CuH capped with a monolayer of pyridine. This was modeled using the same five-layer $CuH_{0.75}$ slab as for the hydroxyl-terminated structure but with the hydroxyls replaced by pyridine coordinated to copper. Pyridine usually coordinates via the nitrogen atom in an η^1-mode (as seen in $[Cu(C_5H_5N)_4(SO_3CF_3)_2]$[50]); however, η^6-coordination is also known on metal single-crystal surfaces at low coverage[51] and in complexes, for example, tricarbonyl(η^6-pyridine)-chromium(0).[52] Test calculations for η^6-coordination resulted in the pyridine "drifting-off" into the vacuum gap. A calculation with η^1-coordination of the pyridine to a surface hydrogen atom caused the pyridine to move to the nearest copper atom. Thus, the most likely geometry is that pyridine is oriented vertically to the surface and η^1-coordinated through the nitrogen atom to a copper atom.

The unit cell of the $CuH_{0.75}$ slab has two surface copper atoms. Steric considerations only allow one pyridine per unit

DOI: 10.1021/ic5027009
Inorg. Chem. 2015, 54, 2213−2220

cell; however, this results in intermolecular contacts of less than 2 Å, and the pyridine spectrum is significantly modified. Generating a 2 × 2 × 1 supercell with one pyridine per unit cell eliminates the close contacts and results in a pyridine spectrum that resembles that of the bulk. Comparison of the calculated and observed spectra (Supporting Information, Figure S10a,b) shows that the ratio of pyridine to CuH is too large in the model and also that we are unable to simultaneously model the narrow line width of the pyridine and the very broad line width of the CuH (Figure 6). By extracting the individual spectral contributions of pyridine and CuH and scaling the relative contributions, both problems could be overcome.

The process is shown in Supporting Information, Figure S10c–e, and the result is shown in Figure 11. It can be seen

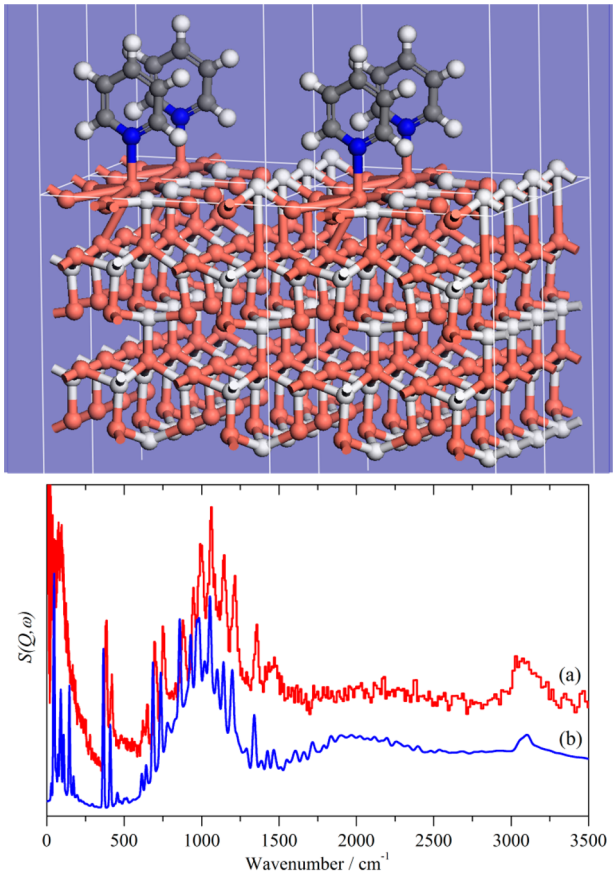

Figure 11. INS spectrum of (a) CuH/pyridine and (b) that generated from the pyridine-terminated $CuH_{0.75}$ slab shown above.

that the agreement is excellent, strongly supporting the model. The results indicate a CuH/pyridine ratio of ~7:1, which is in reasonable agreement with the 5:1 ratio found necessary to process the total scattering ND data of the same sample. Both results reinforce the conclusion from X-ray data that the particle size is very small and hence that the overall surface area is large. A simple cuboid of 12 × 12 × 15 Å, to give an ~17 Å diameter nanoparticle, has a ratio of surface to bulk copper atoms of ~1:1; thus, assuming one pyridine per eight copper atoms (as indicated by the need for a 2 × 2 cell), this would give a CuH/pyridine ratio in agreement with experiment.

Our calculations show that, for stoichiometric CuH, there should be infrared and Raman active modes at 883 and 894 cm^{-1} and a weakly Raman active mode at 1070 cm^{-1}, although almost all previous attempts to record infrared or Raman spectra from CuH prepared by routes (1) or (3) have failed.[15,21,22] If the products were non-stoichiometric, as is usually the case, and hence metallic, this would account for the failure to observe infrared or Raman spectra. The only credible observation of a Cu–H stretch mode is from ref 23. This work reported a broad, structured feature in the infrared spectrum that extended from 720 to 1180 cm^{-1}. The large width was attributed to strong anharmonicity in the sample; however, our work shows that, while anharmonicity is present, it is not unusually large: ω_e = 1122 cm^{-1} and $2\omega_e x_e$ = 66 cm^{-1}, that is, $\omega_e x_e \approx 3\%\ \omega_e$. Inspection of their data shows that the range from 720 to ~1000 cm^{-1} decreased with time at a different rate to that of the ~1000 to 1180 cm^{-1} range. The product was not completely dried, and comparison with Figure 2a–c and the infrared spectra[53] of liquid water and ice strongly suggests that the 720 to 1000 cm^{-1} feature is actually the librational modes of the water solvation shell. The higher energy peaks at ~1040 and 1120 cm^{-1} do occur in the correct region for CuH; however, our calculations indicate that the infrared active modes occur at significantly lower energy. The surface hydroxyl layer does have bending modes in this region, and it is possible that the modes are associated with these OH flexures rather than with bulk CuH.

CONCLUSIONS

CuH is still of current interest as shown by a recent report that details a new preparation in aqueous solution facilitated by sonochemical methods.[16] The evidence suggests, for CuH synthesized by aqueous routes, a model consisting of relatively large (several hundred nanometers) nanoparticles of a poorly crystalline core of nonstoichiometric CuH capped with a monolayer of hydroxyls and surrounded by water molecules. (Although not investigated here, this is also probably true of the sonochemical synthesis.) This model is similar to that found for $PdO{\cdot}H_2O$[41] and $Al_2O_3{\cdot}xH_2O$,[44] except with a CuH core rather than a metal oxide core. For CuH/pyridine, a model of a very small, poorly crystalline core of nonstoichiometric CuH capped with a monolayer of pyridine is indicated.

The difference in the surface chemistry of CuH formed by aqueous and nonaqueous routes provides a rationale for their differing behaviors. Cu(I) forms a wide variety of complexes of the type $(CuLX)_n$ where L = N or P donor, X = Cl, Br, I, and n = 1–6.[54] Thus, the solubility of CuH/pyridine in a variety of donor solvents[15] (alkyl sulfides, alkylphosphines, and phosphites) is not surprising. In contrast, the aqueous routes result in a material with a chemically bound hydroxyl layer, rather than a coordinated donor layer, effectively preventing dissolution in organic solvents. The much smaller particle size of CuH/pyridine means that a large fraction of the copper atoms will be coordinated by a donor, and this probably assists dissolution.

Perhaps the most surprising feature of CuH is that it is formed at all. Cu(I) readily disproportionates to Cu(0) and Cu(II) unless stabilized by soft donors. From ternary transition metal hydrides[55] there is evidence that hydride ion can function in a similar fashion, as the large polarizability of the hydride ion, that is, the "low resistance to a deformation of its electron density",[56] distributes electron density away from the central atom, and a similar effect is probably operational here also.

Functionalization and optimization of nanoparticles by manipulation of the surface layer is a topic of considerable interest,[57] as it potentially provides a means to tailor the

DOI: 10.1021/ic5027009
Inorg. Chem. 2015, 54, 2213–2220

properties of the system. This work provides a particularly clear example of how the nature of an adsorbed layer on a nanoparticle surface determines the properties.

■ ASSOCIATED CONTENT

Supporting Information

Synthetic procedures, dispersion curves, and electronic density of states of CuH and $CuH_{0.75}$, XRD and INS spectra of CuH prepared by both routes, and INS spectra of reference materials. This material is available free of charge via the Internet at http://pubs.acs.org.

■ AUTHOR INFORMATION

Corresponding Author

*E-mail: stewart.parker@stfc.ac.uk.

Notes

The authors declare no competing financial interest.

■ ACKNOWLEDGMENTS

The STFC Rutherford Appleton Laboratory is thanked for access to neutron beam facilities. Computing resources (time on the SCARF computer used to perform the CASTEP calculations) was provided by STFC e-Science facility.

■ REFERENCES

(1) Würtz, A. *C. R. Hebd. Seances Acad. Sci.* **1844**, *18*, 702.
(2) Burzyńska, L.; Stoch, J.; Zembura, Z. *Solid State Ionics* **1990**, *38*, 179.
(3) Burzyńska, L.; Karp, J.; Zembura, Z. *Solid State Ionics* **1994**, *73*, 35.
(4) Vaškelis, A.; Juškėnas, R.; Jačiauskienė, J. *Electrochim. Acta* **1998**, *43*, 1061.
(5) Elliott, A. J.; Sakakini, B.; Tabatabaei, J.; Waugh, K. C.; Zemicael, F. W.; Hadden, R. A. *J. Chem. Soc., Faraday Trans.* **1995**, *91*, 3659.
(6) Fitzsimons, N. P.; Jones, W.; Herley, P. J. *Catal. Lett.* **1992**, *15*, 83−94.
(7) Tanaka, H.; Yamaguchi, Y.; Sumida, S.-I.; Kuroboshi, M.; Mochizuki, M.; Torii, S. *J. Chem. Soc., Perkin Trans.* **1999**, *1*, 3463.
(8) Rendler, S.; Oestreich, M. *Angew. Chem., Int. Ed.* **2007**, *46*, 498.
(9) Deutsch, C.; Krause, N.; Lipshutz, B. H. *Chem. Rev.* **2008**, *108*, 2916.
(10) Churchill, M. R.; Bezman, S. A.; Osborn, J. A.; Wormald, J. *Inorg. Chem.* **1972**, *11*, 1818.
(11) Fitzsimons, N. P.; Jones, W.; Herley, P. J. *J. Chem. Soc., Faraday Trans.* **1995**, *91*, 713.
(12) Warf, J. C.; Feitknecht, W. *Helv. Chim. Acta* **1950**, *33*, 613.
(13) Dasgupta, M.; Mahanti, M. K. *Oxid. Commun.* **2010**, *33*, 88.
(14) Wiberg, E.; Henle, W. *Z. Naturforsch.* **1952**, *7b*, 250.
(15) Dilts, J. A.; Shriver, D. F. *J. Am. Chem. Soc.* **1968**, *90*, 5769.
(16) Hasin, P.; Wu, Y. *Chem. Commun.* **2012**, *48*, 1302−1304.
(17) Müller, H.; Bradley, A. J. *J. Chem. Soc.* **1926**, 1669.
(18) Goedkoop, J. A.; Andersen, A. F. *Acta Crystallogr.* **1955**, *8*, 118.
(19) Fukai, Y. *The Metal-Hydrogen System: Basic Bulk Properties;* Springer-Verlag: Berlin, 1993; Chapter 1.
(20) Burtovyy, R.; Tkacz, M. *Solid State Commun.* **2004**, *131*, 169.
(21) Mikheeva, V. I.; Mal'tseva, N. N. *J. Struct. Chem.* **1963**, *4*, 643.
(22) Golovanova, A. I.; Minaeva, N. A.; Mal'tseva, N. N. *Russ. J. Inorg. Chem.* **1995**, *40*, 1061.
(23) Korzhavyi, P. A.; Soroka, I. L.; Isaev, E. I.; Lilja, C.; Johansson, B. *Proc. Natl. Acad. Sci. U.S.A.* **2012**, *109*, 686−689.
(24) Thornton, D. A. *Coord. Chem. Rev.* **1990**, *104*, 251.
(25) Soroka, I. L.; Tarakin, N. V.; Korzhavyi, P. A.; Stepanenko, V.; Jonsson, M. *CrystEngComm* **2013**, *15*, 8450−8460.
(26) http://www.isis.stfc.ac.uk/instruments/sandals/.
(27) http://www.isis.stfc.ac.uk/.
(28) http://www.isis.stfc.ac.uk/instruments/sandals/data-analysis/gudrun8864.html.
(29) Hannon, A. C.; Howells, W. S.; Soper, A. K. *Inst. Phys. Conf. Ser.* **1990**, *107*, 193.
(30) Farrow, C. L.; Juhás, P.; Liu, J. W.; Bryndin, D.; Božin, E. S.; Bloch, J.; Proffen, Th.; Billinge, S. J. L. *J. Phys.: Condens. Matter* **2007**, *19*, 335219.
(31) Mitchell, P. C. H.; Parker, S. F.; Ramirez-Cuesta, A. J.; Tomkinson, J. *Vibrational spectroscopy with neutrons, with applications in chemistry,biology, materials science and catalysis;* World Scientific: Singapore, 2005.
(32) Parker, S. F.; Fernandez-Alonso, F.; Ramirez-Cuesta, A. J.; Tomkinson, J.; Rudic, S.; Pinna, R. S.; Gorini, G.; Fernández Castañon, J. *J. Phys. Conf. Ser.* **2014**, *554*, 012003.
(33) http://www.isis.stfc.ac.uk/instruments/maps/.
(34) Parker, S. F.; Lennon, D.; Albers, P. W. *Appl. Spectrosc.* **2011**, *65*, 1325−1341.
(35) Segall, M. D.; Lindan, P. J. D.; Probert, M. J.; Pickard, C. J.; Hasnip, P. J.; Clark, S. J.; Payne, M. C. *J. Phys. Condens. Mater.* **2002**, *14*, 2717.
(36) Clark, S. J.; Segall, M. D.; Pickard, C. J.; Hasnip, P. J.; Probert, M. J.; Refson, K.; Payne, M. C. *Z. Kristallogr.* **2005**, *220*, 567.
(37) Morris, A. J.; Nicholls, R. J.; Pickard, C. J.; Yates, J. R. *Comput. Phys. Commun.* **2014**, *185* (5), 1477.
(38) Refson, K.; Tulip, P. R.; Clark, S. J. *Phys. Rev. B* **2006**, *73*, 155114.
(39) http://accelrys.com/products/materials-studio/.
(40) Ramirez-Cuesta, A. J. *Comput. Phys. Commun.* **2004**, *157*, 226.
(41) Parker, S. F.; Refson, K.; Hannon, A. C.; Barney, E.; Robertson, S. J.; Albers, P. *J. Phys. Chem. C* **2010**, *114*, 14164.
(42) Spencer, E. C.; Ross, N. L.; Parker, S. F.; Woodfield, B. F.; Boerio-Goates, J.; Smith, S. J.; Olsen, R. E.; Kolesnikov, A. I.; Navrotsky, A.; Ma, C. *J. Phys.: Condens. Matter* **2011**, *23*, 205303.
(43) Spencer, E. C.; Ross, N. L.; Parker, S. F.; Kolesnikov, A. I.; Woodfield, B. F.; Woodfield, K.; Boerio-Goates, J.; Navrotsky, A. *J. Phys. Chem. C* **2011**, *115*, 21105−21112.
(44) Spencer, E. C.; Huang, B.; Parker, S. F.; Kolesnikov, A. I.; Ross, N. L.; Woodfield, B. F. *J. Chem. Phys.* **2013**, *139*, 244705.
(45) Lundie, D. T.; McInroy, A. R.; Marshall, R.; Winfield, J. M.; Mitchell, C.; Dudman, C. C.; Jones, P.; Parker, S. F.; Lennon, D. *J. Phys. Chem. B* **2005**, *109*, 11592−11601.
(46) Parker, S. F.; Bennington, S. M.; Ramirez-Cuesta, A. J.; Auffermann, G.; Bronger, W.; Herman, H.; Williams, K. P. J.; Smith, T. *J. Am. Chem. Soc.* **2003**, *125*, 11656−11661.
(47) Nakamoto, K. *Infrared and Raman Spectra of Inorganic and Coordination Compounds, Part A: Theory and Applications in Inorganic Chemistry,* 5th ed.; John Wiley and Sons: New York, 1997; p 12.
(48) Balan, E.; Lazzeri, M.; Delattre, S.; Méheut, M.; Refson, K.; Winkler, B. *Phys. Chem. Miner.* **2007**, *34*, 621−625.
(49) Soroka, I. L.; Shchukarev, A.; Jonsson, M.; Tarakin, N. V.; Korzhavyi, P. A. *Dalton Trans.* **2013**, *42*, 9585.
(50) Noro, S.-I.; Fukuhara, K.; Sugimoto, K.; Hijikata, Y.; Kubo, K.; Nakamura, T. *Dalton Trans.* **2013**, *42*, 11100.
(51) Zhong, Q.; Gahl, C.; Wolf, M. *Surf. Sci.* **2002**, *496*, 21−32 and references therein.
(52) Draper, S. M.; Byrne, J. J.; Breheny, C. J.; Long, C.; Low, J. N. *Acta Crystallogr., Sect. C: Cryst. Struct. Commun.* **1994**, *50*, 1669−1671.
(53) Arakawa, M.; Kagi, H.; Fukazawa, H. *Astrophys. J., Suppl. Ser.* **2009**, *184*, 361−365.
(54) Greenwood, N. N.; Earnshaw, A. *Chemistry of the Elements;* Pergamon Press: Oxford, U.K., p 1387.
(55) Parker, S. F. *Coord. Chem. Rev.* **2010**, *254*, 215−234.
(56) Olofsson-Mårtensson, M.; Häussermann, U.; Tomkinson, J.; Noréus, D. *J. Am. Chem. Soc.* **2000**, *122*, 6960−6970.
(57) Schoenbaum, C. A.; Schwartz, D. K.; Medlin, J. W. *Acc. Chem. Res.* **2014**, *47*, 1438−1445.

DOI: 10.1021/ic5027009
Inorg. Chem. 2015, 54, 2213−2220